Rectification of the Channelrhodopsin Early Conductance

Dietrich Gradmann,[†][*] André Berndt,[‡] Franziska Schneider,[‡] and Peter Hegemann[‡]

[†]A.-v.-Haller-Institut der Universität, Göttingen, Germany; and [‡]Institute for Biology, Experimental Biophysics, Humboldt-Universität zu Berlin, Berlin, Germany

ABSTRACT   We analyzed the nonlinear current-voltage relationships of the early conducting state of channelrhodopsin-2 expressed in *Xenopus* oocytes and human embryonic kidney cells with respect to changes of the electrochemical gradients of H^+, Na^+/K^+, and Ca^{2+}/Mg^{2+}. Several models were tested for wild-type ChR2 and mutations at positions E90, E123, H134, and T159. Voltage-gating was excluded as cause for the nonlinearity. However, a general enzyme kinetic model with one predominant binding site yielded good fits throughout. The empty site with an apparent charge number of about -0.3 and strong external cation binding causes some inward rectification of the uniport function. Additional inward rectification is due to asymmetric competition from outside between the transported ion species. Significant improvement of the fits was achieved by introducing an elastic voltage-divider formed by the voltage-sensitive barriers.

INTRODUCTION

Channelrhodopsin-2 (ChR2) of *Chlamydomonas reinhardtii* and VChR1 of *Volvox carteri* are prototypes of light-gated channels that initiate vision in phototactic algae (1), and they are used as tools to trigger action potentials by light-induced depolarizations in ChR2-transfected cells (2,3). The current-voltage relationship $I(E)$ of ChR is crucial for its function. This study provides and explores a quantitative framework for understanding of the nonlinear $I(E)$ of ChR2 on a molecular level. In general, this is a complicated task, because ChR2 has several conducting states (4,5) which are subjected to voltage-sensitive, temporal inactivation (gating). However, part of this task could be performed here, focusing on the active (open) conformation of one particular conducting state.

In more detail, there is consensus about the simplified ChR photocycle (Fig. 1 A), with two open and two closed states (4–6). Given this reaction scheme, the irreversible transition from C_2 to C_1 in Fig. 1 A means that in the beginning of illumination of dark-adapted ChR2, the conductance observed can be assigned to the open state O_1 exclusively, irrespective of its life time. This conductance is determined here by back extrapolation of the current relaxation between peak and plateau to time zero of illumination, as indicated by the instantaneous current I_0 in Fig. 1 B.

Single-channel recordings of ChR2 are not available because of the small single-channel conductance. However, a ChR single-channel current of ~15 fA in physiological standard conditions (-100 mV, 100 mM external Na^+, and pH_e 7.5) has been estimated from in situ recordings of *Chlamydomonas* cells (7) and was confirmed by more recent studies (8,9). This reference current of 15 fA is used here to convert macroscopic photocurrents from ChR-2 populations in *Xenopus* oocytes and human embryonic kidney (HEK) cells to microscopic currents through an individual ChR-2 molecule.

In symmetric substrate conditions, steady-state $I(E)$ of ChR2 shows inward rectification, which is traditionally explained by an activity, $a(E)$ $0 < a < 1$, that increases with negative voltages. In contrast, Feldbauer et al. (8) suggested that the voltage-dependent transport function itself shows inward rectification due to an asymmetric Eyring barrier (Fig. 2 B). However, fast voltage-dependent blockage by cytoplasmic Mg^{2+}, as in inward rectifying K^+ channels (for review see e.g. (10)), could not be ruled out so far. We show here that neither block by cytoplasmic Mg^{2+} nor an asymmetric barrier of the transport function do account for the observed inward rectification of ChR2.

Our analysis uses the fundamental formalism of enzyme kinetics, as it subsumes channel-mediated permeation of ions through the membrane as well. (Our terminology occasionally switches between general enzyme kinetics and *channology*; e.g., active/*open*, inactive/*closed*, competitive inhibition/*blockage*, inactivation/*gating*, activity/*conductance, current*, etc.) We use a reaction scheme that allows kinetic modeling of the current-voltage relation of the ChR-currents under different ionic conditions and to determine the rate constants of the reaction scheme from experimental data. This treatment explains ChR2 inward-rectification as a combination of a nonlinear transport function and asymmetric competition between several cation species.

The model

We start from the general four-state model for enzymatic uniport of an ionic substrate S through lipid membranes (mother scheme in Fig. 1 C). It reflects a predominant binding site E, which can switch its orientation, empty or loaded, between the cytoplasmic side c and the external side e, yielding the corresponding four states E_c, E_e, ES_c
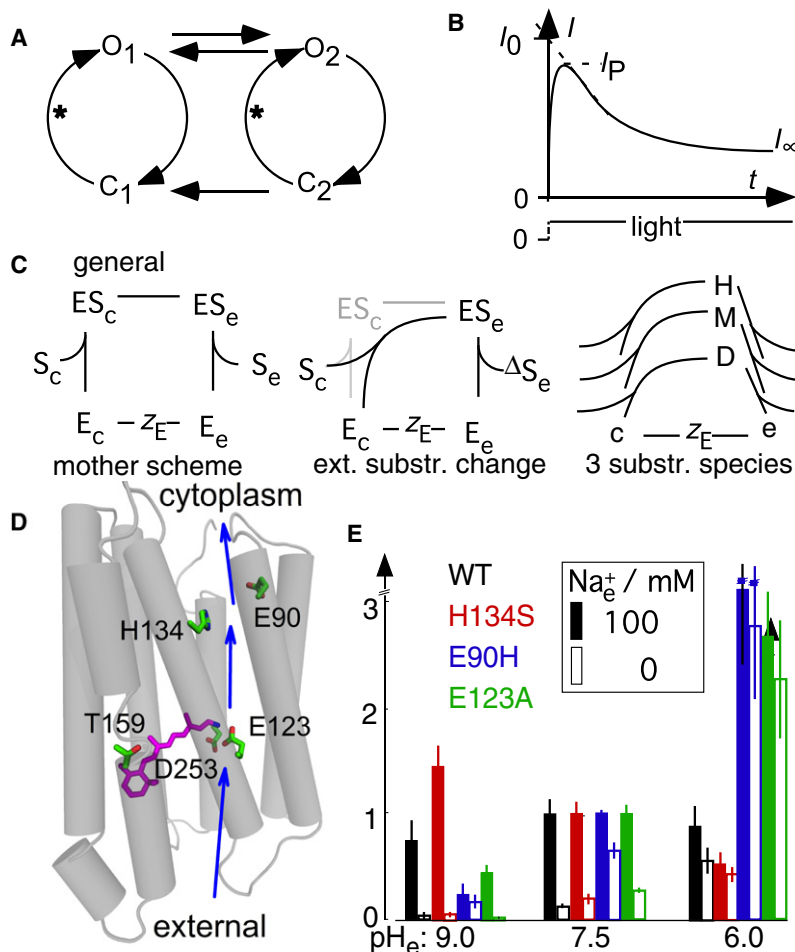
FIGURE 1 Background information. (*A*) ChR photocycle with two serial open states O_1 and O_2, and two closed states C_1 and C_2. (*B*) Typical time course of photocurrent upon a rectangular pulse of bright light; extrapolation of the current relaxation from peak to plateau to time zero, yields I_0, which is assigned to the early conducting state O_1 exclusively. (*C*) General reaction scheme for enzymatic (*E*) translocation of ionic substrates S; z_E: charge number of empty binding site; left: mother scheme, middle: reduction of four-state mother scheme (*light gray*) to three-state scheme (*black*) for possible parameter identification from experimental $I(E)$ curves with external substrate changes; right: scheme for treating three competing substrates H (H^+), M (K^+ and Na^+), and D (Ca^{2+} and Mg^{2+}) simultaneously. (*D*) Three-dimensional computer model of ChR2, based on the coordinates of *Halobacterium salinarum* bacteriorhodopsin [21] and drawn with Pymol (Schrödinger); highlighted amino acids are expected to play a major role in ion translocation; retinal moiety is marked; arrows: conjectural path of ions from external to cytoplasmic space. (*E*) Photocurrents survey from ChR2 WT and three mutants, measured at -100 mV in presence and absence of 100 mM external Na^+, at pH_e 9, 7.5, and 6; means $\pm$ SE from $n = 3$–9 independent experiments, normalized to recording at pH_e 7.5 with 100 mM external Na^+.

and ES_e. The charge number of the empty binding site, z_E, is essential for the voltage-sensitivity of the system [11,12].

For channels with several binding sites in series, reorientation in Fig. 1 *C* needs to be explained: loaded site means that all sites are occupied, and empty site means that all sites are occupied as well, except the most external one, E_e, or the most cytoplasmic one, E_c, [13].

For the general four-state model for uniport (Fig. 1 *C*, *left*), the rate constants can theoretically be determined by analysis of the nonlinear current-voltage relationships, recorded with different substrate concentrations on both sides of the membrane [14]. However, if the substrate concentration can only be changed outside as in our oocyte experiments, only the parameters of a three-state model can be determined, where cytoplasmatic binding/debinding and reversible orientation of the loaded binding site are lumped into one reversible reaction step [12,15]. This reduction from a four-state model to a three-state model is illustrated in Fig. 1 *C* (center).

The right panel in Fig. 1 *C* shows the extension of this three-state model for uniport to a five-state model for competitive transport of the three substrates H (H^+), M ($K^+ + Na^+$), and D ($Ca^{2+} + Mg^{2+}$) where all three cycles

share the reorientation, c–e, of the empty binding site. Summing $K^+ + Na^+$ up to monovalent cations, M, is justified by the findings that K^+ and Na^+ contribute to the photocurrents quite similarly [9,15,16]. Based on similar changes of the reversal voltages upon changes in external Mg^{2+} or Ca^{2+} concentrations [17], these ions may be summarized as divalent cations D.

Microscopic reversibility dictates that, for instance, in the closed uniport H^+-cycle with the three states c, e, and H, only five of the six fundamental rate constants (k_{ec}^0, k_{ce}^0, k_{cH}^0, k_{Hc}^0, k_{He}^0, and k_{eH}^0) are independent because of $k_{ce}^0 k_{eH}^0 k_{Hc}^0 = k_{cH}^0 k_{He}^0 k_{ec}^0$. More general, for a substrate S we arbitrarily chose k_{eS}^0 to be the dependent one with

$$k_{eS}^0 = \frac{k_{ec}^0 k_{cS}^0 k_{Se}^0}{k_{Sc}^0 k_{ce}^0}. \qquad (1)$$

Altogether, our general model, reduced for sole external substrate changes, comprises 12 independent parameters: nine substrate-specific rate constants (k_{cS}^0, k_{Sc}^0, and k_{Se}^0 for each substrate), two substrate-unspecific ones (k_{ce}^0 and k_{ce}^0), and the apparent charge number z_E of the empty binding site.
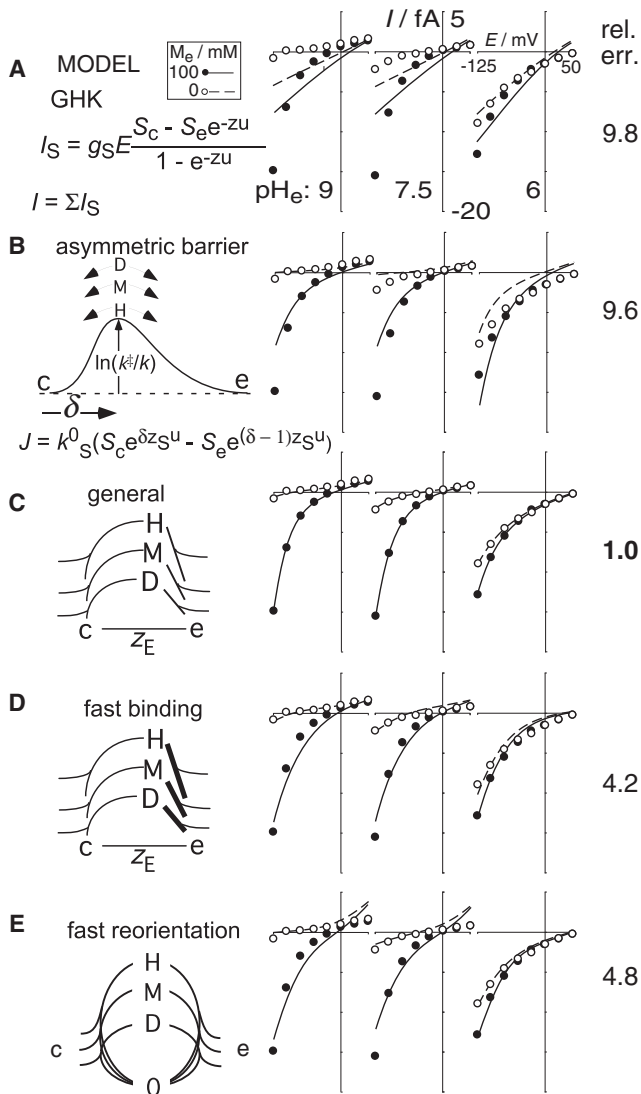
FIGURE 2 Fits of theoretical current-voltage relationships (*curves*) of five models (*A–E*) to experimental data (*dots*), recorded at different pH_e in zero (*open symbols, dashed curves*) and 100 mM (*solid symbols and curves*) external Na^+. Sketches in the left column indicate the various models; rel. err. in right column indicates the fit quality. Example E123Q1 out of five independent experiments with E123Q. Panels *C–E* already account for the result in Fig. 3 *A*, saying that $I(E)$ is independent of the cytoplasmic concentration of divalent cations, and for the elastic voltage profile, mentioned below.

The conversion of the fundamental rate constants k^0 to apparent ones, k, as functions of substrate concentrations and voltage is described by Eq. S9 and Eq. S10 in the Supporting Material. The algorithm for the current-voltage relationship through this five-state reaction scheme is given by the chapter, General enzyme kinetic model, at the same place.

For this study, we used wild-type (WT) ChR-2 and variants that were mutated by the amino acid residues that were either known or suggested to be critical for ion conductance (E123, T159) [18,19] and for selectivity (E90,

H134)[9,20]. These amino acids are marked in the three-dimensional computer model (Fig. 1 *F*) that is derived from x-ray structures of other microbial rhodopsins [21].

MATERIALS AND METHODS

Experimental

Voltage clamp experiments on heterologously expressed ChR2 were carried out in *Xenopus* oocytes as described [15,22] and in HEK cells as described by [15,22]. Using fixed 3 M KCl agar bridges for the external electrode, changes of the liquid junction voltages upon a medium change were <2 mV according to [23], and considered small enough to be ignored. Cytoplasmic free cation concentrations (in mM) were ≈ 2 Mg^{2+}, <0.001 Ca^{2+}, ≈ 110 K^+, ≈ 10 Na^+, pH_c 7.3 in oocytes [24] and 110 Na^+, <0.001 Ca^{2+} (10 EGTA, 2 total Ca^{2+}), 5 K^+, 0.2, 2 or 20 Mg^{2+}, pH_c 7.2 in HEK cells. If not mentioned otherwise, the bath for both systems contained 100 *N*-methyl-d-glucosamide$^+$ or Na^+, 2 Ca^{2+}, 2 Mg^{2+}, 0 or 2 K^+, pH_e 9.0, 7.5 or 6.0 buffered with 10 Tris or Hepes. Anions are irrelevant here because they are not conducted by ChR-2 [17]. Usually photocurrents were studied 3–7 days after RNA injection. A 75 W Xenon lamp (Jena-Instruments, Jena, Germany) combined with a fast shutter (Uniblitz model T132, Vincent Associates, Rochester, NY) was used for light pulses. Blue light was selected with a dichroic mirror reflecting 450–490 nm light through the objective onto the sample. 100% light intensity corresponded to 4.5×10^{21} photons m^{-2} s^{-1} at the cell surface.

Theoretical

Algorithms

Detailed descriptions of the numerical treatment of the five transport models used and the applied fitting strategy are given in the Supporting Material. The rate constants of the model (e.g., from Table S1) were converted into potential profiles (see Fig. 6 *C*, Fig. S3) using the general relationship

$$E = \left(\frac{RT}{F}\right) \ln\left(\frac{k^{\ddagger}}{k}\right), \qquad (2)$$

where E marks the voltage ordinate, R, T, and F have their usual thermodynamic meaning, $k^{\ddagger} \approx 6.25 \times 10^{12}$ s^{-1} is the frequency factor at room temperature, and k is a rate constant in s^{-1}. Fig. S3 *B* illustrates this conversion for an arbitrary substrate S (H, M, or D).

Scaling and normalizing

Current voltage relationships from different cells, i.e., from different expression levels are normalized to the reference photocurrent I_{ref} at −100 mV, pH_e 7.5 in the presence of 100 mM external Na^+, and 1 mM Ca^{2+}, which was routinely recorded to check the stability of the preparation. Using the mentioned reference value (15 fA) for the steady-state current through the two states of one WT ChR2 molecule, the initial current through the state O_1 could also be expressed in absolute terms. Current recordings of the mutants were also normalized by their steady-state current at these reference conditions, and finally rescaled by the ratio of the mean initial currents I_{0Mu}/I_{0WT}. Similar expression of WT and the various mutants is assumed for this calibration.

Numerical, plots, and markers

The custom-tailored software was written in Turbo-Pascal, and is available on request. For the sake of transparency, identical scales in multiple-panel figures are lettered only once explicitly. Individual experiments are

identified by final numbers; e.g., E90H2 means, it was the second experiment out of a series of independent, successful experiments with E90H.

RESULTS AND DISCUSSION

For screening purposes, we initially measured instantaneous photocurrents I_0 (see Fig. 1 B) at pH 9, 7.5, and 6, at -100 mV in the absence and presence of 100 mM external Na^+. The results in Fig. 1 E readily showed that the H/Na selectivity severely differs in many of the mutants tested. For example, the Na^+-induced inward currents were large in WT and H134S but small in E90H and E123A. Surprisingly, different substitutions at a single position, for example E123, resulted in quite different selectivities. These initial observations motivated us to study ion selectivity in more detail.

Comparison of models and fits

Before the detailed comparison of the mutants, we applied five models to one experimental data set from the ChR2-E123Q, which shows Na-dependence larger than WT (Fig. 2). E123 contributes to the complex anion that counterbalances the positive charge of the protonated retinal Schiff base ($RSBH^+$) (18). Second, this residue is responsible for the voltage sensitivity of the photocycle and the gating of the channel (19).

The most familiar Goldman-Hodgkin-Katz (GHK) model (Fig. 2 A) fails to describe the experimental data, mainly because of the small curvature of the theoretical $I(E)$ relationships. Fits with a single, asymmetric barrier (Fig. 2 B) do describe the inward rectifying $I(E)$ data better than GHK. However, several details also are not well reproduced by this model. Its fundamental assumption of independent movement of the various cations is unrealistic here. Furthermore, the single barrier model would exclude any collisions between the ion and its environment during its travel through the membrane.

The general model of Fig. 1 C provided the best fits of all sets of $I(E)$ curves such as in Fig. 2 C. Because the difficulty of this model is the large number of 12 free parameters, we tested reduced models with only nine free parameters (Fig. 2, D and E, for details see the Supporting Material) as possible alternatives. In particular, the fast-binding version (Fig. 2 D) was a good candidate to account for the ChR inward rectifying $I(E)$ characteristics (25), as it allowed the analysis of reversal voltages in a competitive transport system (17). In fact, fits with this fast-binding model are significantly better (Fig. 2 D) than those with the one asymmetric barrier model (Fig. 2 B). However, too small curvature of the inward rectifying characteristics in the presence of 100 mM external Na^+, seems to be a systematic error with this fast-binding model. The fast-reorientation model (Fig. 2 E) shows fits of similar quality as the fast-binding model D. Systematic errors of the fast-reorientation

model are too large outward currents compared to the experimental data. We turn now to some details that have not been mentioned but considered so far.

The role of divalent cations, D

The main body of experimental data in this study consists of sets of six experimental $I(E)$ curves at different concentrations of external H and M, as in the example in Fig. 2. Because models with only these two substrates failed to provide good fits, a third substrate was implemented. From selectivity studies (17) the additional physiologically relevant substrates were known to be Ca^{2+} and Mg^{2+} (D). The role of D was already implemented in the fits for Fig. 2. Explicit results of the role of cytoplasmic and external D are given in this section.

We have tested the possible effect of cytoplasmic Mg^{2+} because cytoplasmic Mg^{2+} is known to cause inward rectification in K^+ channels (for review see (10)). Because the cytoplasmic ion composition in *Xenopus* oocytes cannot be controlled sufficiently by the experimenter, HEK cells were employed for these experiments.

The results from these HEK cell experiments are illustrated in Fig. 3 A. Within an accuracy of ~5%, these $I(E)$ curves (normalized to the reference current at -75 mV), from cells with 2 or 20 mM cytoplasmic Mg^{2+} do coincide between -75 and $+50$ mV at pH_e 7.5 (Fig. 3 A). This coincidence holds also at pH_e 9 and pH_e 6, as shown by the unframed inset in Fig. 3 A. In addition, this inset in Fig. 3 A shows that the inward rectifying curvature of $I(E)$—expressed by the ratio of the current amounts at $+50$ mV over -75 mV—increases with the external H^+ concentration.

Before the lack of the effect of cytoplasmic Mg^{2+} was known, initial analysis included its action as an additional free parameter, which falsely resulted in a clear preference for the fast-reorientation model (Fig. 2 E), and the numerical solutions were very robust with respect to alternative start parameters. However, when the insensitivity of the $I(E)$ curves to cytoplasmic D (Fig. 3 A) became evident, and when this insensitivity was implemented into the models by simultaneous fits with different (2 and 20 mM) cytoplasmic D, this preference vanished. This result is reflected by the similar error in panel D and E of Fig. 2, and lead to the conclusion that both these simplifications are equally inferior, compared to the general model Fig. 2 C.

The possible impact of *external* D on the experimental $I(E)$ curves was investigated with *Xenopus* oocytes again (Fig. 3 B). For these experiments we employed—in addition to ChR2 WT—two variants (H134R and T159C) with large photocurrents. ChR2-H134R was actually the first mutation we ever made in a ChR (ChR1 and ChR2) because this position reprotonates the RSB in bacteriorhodopsin (pos. D96) (26). Whereas Asp at this position rendered the protein almost totally inactive, the H134R currents can even be higher than from WT (9). The mutant T159C was found

during a color mutant screen. Although the position is close to the β-Ionone ring of the RSB as visualized in Fig. 1 *D*, T159C shows a significantly larger current. Fig. 3 *B* shows the influence of external Ca^{2+} on the *I(E)* curves of WT, T159C, and H134R, by corresponding examples (*left*), which are statistically supported by the right panel, using the ratio *Y* between the currents at -100 mV, in the presence of 10 over 1 mM external Ca^{2+}. In the presence of 100 mM external Na^+ (*solid bars*) this ratio *Y* is significantly decreased; and in the absence of external Na^+ (*open bars*), *Y* is increased. This role of divalent ions in the bath is similar in all three ChR2 variants tested. The analysis below will show that these two effects reflect 1), a simple mass action increase of Ca^{2+} inward currents by increase of external Ca^{2+}concentration (seen in the absence of Na^+ entry), and 2), a competitive occupation of the binding site for predominant Na^+ entry by external Ca^{2+}.

The role of voltage-sensitive partition coefficients

The general model was fitted to 45 standard sets ($n = $ 3–9 sets/variant) of six experimental *I(E)* relationships with three different pH_e values and two different external M concentrations (0 and 100 mM Na^+). The mean reference

currents (at -100 mV at pH_e 7.5 and 100 mM external Na^+) for each ChR were calculated from all *n* cells investigated for scaling absolute currents at the top of the middle (pH_e 7.5) ordinates in the graphs of Fig. 4.

As expected, initial fits by the general model suffered from the large number of free parameters. However, we could improve this model without increasing the number of free parameters, using a modification with respect to the voltage-sensitivity of the rate constants.

Briefly, for the treatment of several (let's say two) voltage-sensitive reaction steps in series, Woodhull (27) introduced an extra independent parameter, the electric distance *d*, that divides the entire transmembrane voltage into two portions. In our case of a predominant binding site at the distance *d* from the cytoplasmic compartment e, the four rate constants for the two serial steps of substrate (S) translocation would have the voltage-sensitivities:

$$k_{cS} = k_{cS}^0 [S]_c \exp\left(\frac{du}{2}\right), \qquad (3a)$$

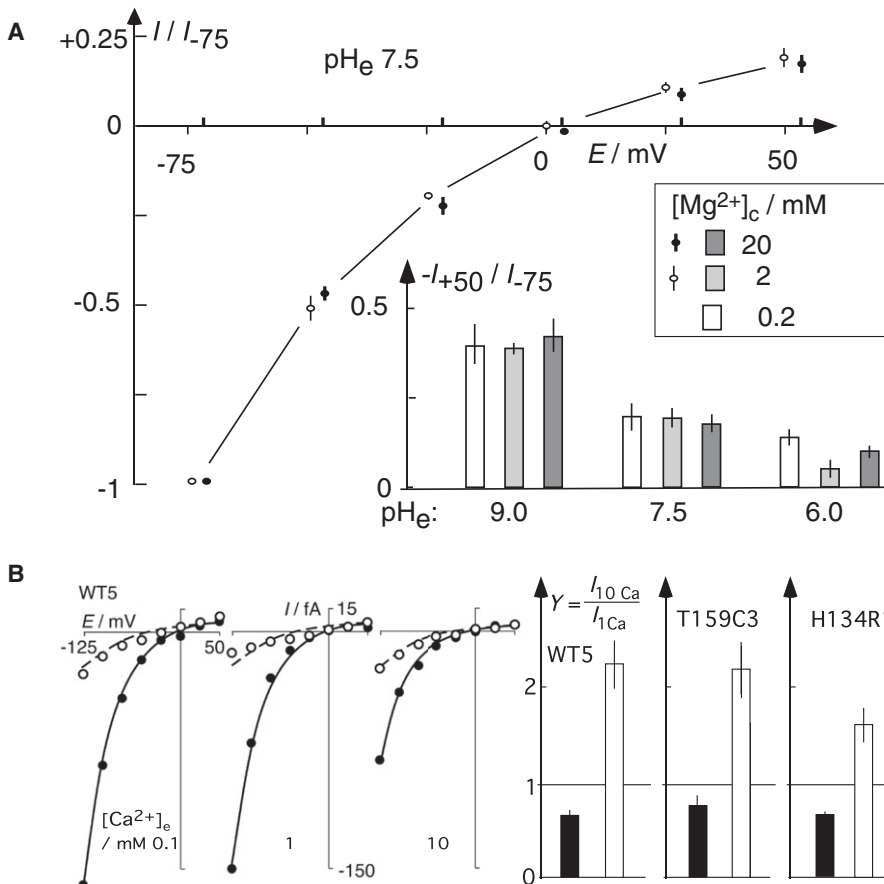$$k_{Sc} = k_{Sc}^0 \exp\left(\frac{-du}{2}\right), \qquad (3b)$$

FIGURE 3   Role of divalent cations, D. (*A*) Cytoplasmic Mg^{2+}; experimental data from HEK cells; main diagram: *I(E)* in 2 mM (*open symbols*) and 20 mM (*solid symbols*) cytoplasmic $[Mg^{2+}]$ at pH_e 7.5, normalized to the reference current at -75 mV; error bars: $\pm$ SE from $n \geq 3$ independent experiments; open inset: Ratio of current amounts from $+50$ mV and -70 mV as phenomenological measure for rectification, recorded with 0.2, 2.0, and 20 mM cytoplasmatic $[Mg^{2+}]$ at three external pH_e 9, 7.5, and 6; error bars: $\pm$ SE of $n \geq 3$ independent recordings; main result: ChR2 rectification is D_c-independent, but H_e-stimulated. (*B*) Impact of D_e in the presence (*solid symbols*) and absence (*open symbols*) of 100 mM Na^+ in the bathing solution at pHe 7.5, experimental data from *X*. oocytes; Left panel: Example fit of general model (Fig. 1 *C*) to experimental data set from WT5, at 0.1, 1, and 10 mM external Ca^{2+} (plus 0.1 mM Mg^{2+} in all solutions); Right panel: statistical support for Ca^{2+}-induced inhibition of Na^+ currents (*black bars*) and Ca^{2+}-induced increase of inward currents in absence of external Na^+ (*open bars*), assessed by comparing instantaneous photocurrents at -100 mV in 1 and 10 mM external Ca^{2+}, as defined by the ratio *Y*. Error bars: $\pm$ SE from $n \geq 3$ independent experiments.
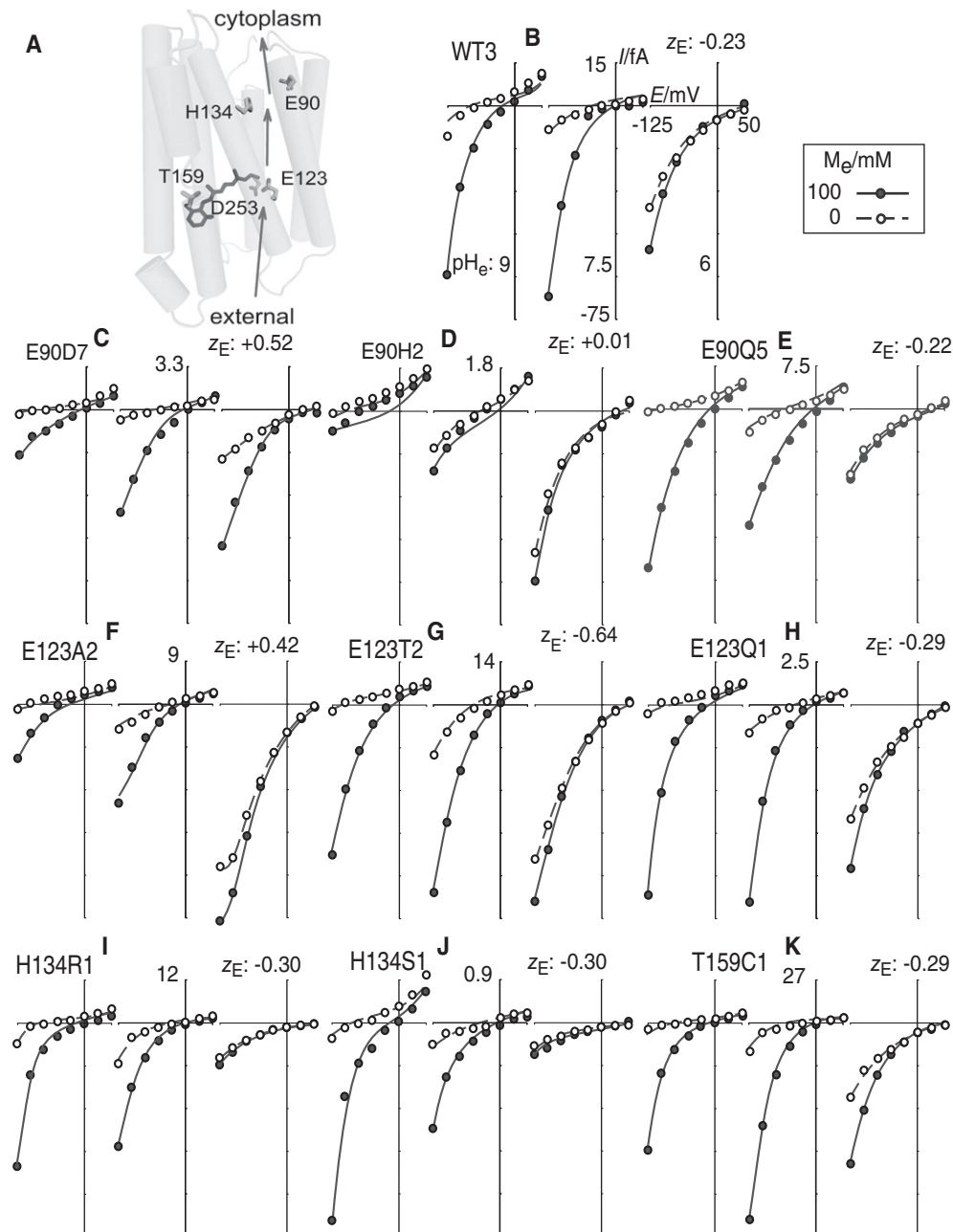
FIGURE 4 Best fits of general model to selected $I(E)$ data sets (pH$_c$ 9, 7.5, and 6, in presence and absence of 100 mM external Na$^+$) of WT and nine mutants tested. (*A*) Three-dimensional model of ChR2 as in Fig. 1 *D*; (*B*) representative examples for WT and each mutant (end number identifies experiment of a series); current scale and resulting z_E (apparent charge of empty binding site) are marked on each panel.

$$k_{Se} = k_{Se}^0 \exp\left(\frac{(1-d)u}{2}\right), \qquad (3c)$$

$$k_{eS} = k_{eS}^0 [S]_e \exp\left(\frac{(d-1)u}{2}\right), \qquad (3d)$$

where the superscript 0 denotes the k value at zero voltage, and $u = EF/(RT)$ is the reduced membrane voltage.

In our first approach, we determined this electrical distance d like in a rigid voltage divider as

$$d = \frac{k_{Se}^0 + k_{eS}^0 \,[S]_e}{k_{Se}^0 + k_{eS}^0 [S]_e + k_{Sc}^0 + k_{cS}^0 [S]_c}, \qquad (4a)$$

according to (28), where $k_{Se}^0 + k_{eS}^0 [S]_e$ and $k_{Sc}^0 + k_{cS}^0 [S]_c$ correspond to two ohmic conductances. Alternatively, a novel, elastic voltage divider was tested, with

$$d = \frac{k_{Se} + k_{eS}[S]_e}{k_{Se} + k_{eS}[S]_e + k_{Sc} + k_{cS}[S]_c}, \quad (4b)$$

where the voltage-sensitive partitioning coefficient d had to be determined iteratively by Eq. 3 and Eq. 4. In fact, fits using Eq. 4b yielded better fits, in general, and the corresponding numerical results are listed in Table S1. More precisely, this superiority was found in 8 of the 10 ChR2 variants tested with the 3–9 data sets from each variant (Fig. 5 A). Only the mutants E90D and E123A yielded significant better fits with the rigid voltage divider using Eq. 4a, compared with the elastic voltage divider using Eq. 4b. Interestingly, these two mutants, E90D and E123A, were the only ones for which the fit algorithm
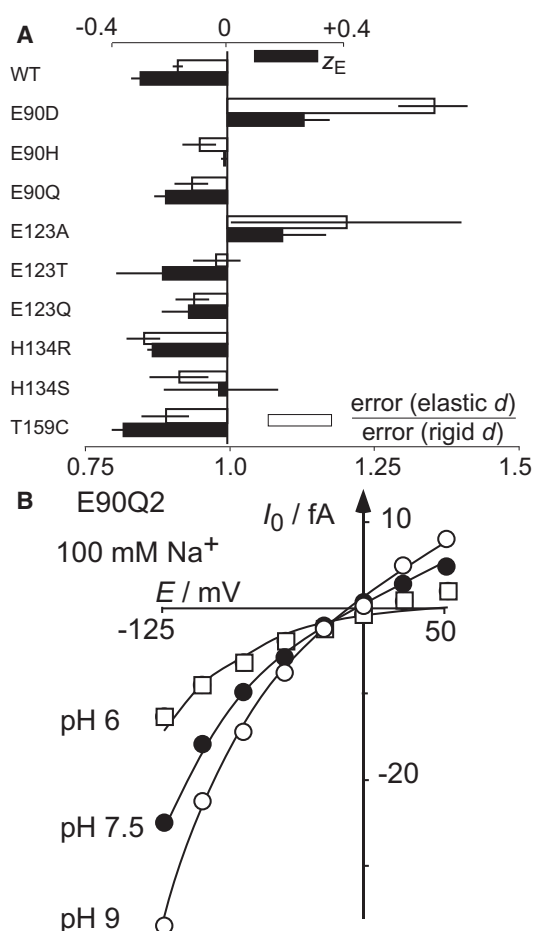

FIGURE 5 Specific results. (A) Charge number, z_E, of the empty binding site, and voltage divider; in general, the general kinetic model (Fig. 1 C) with an elastic, voltage-sensitive voltage-partitioning coefficient, d (Eq. 4b), yields a negative charge number, z_E, of the empty binding site (*upper abscissa* and *solid bars*), and better fits (*smaller errors*) than with a rigid, voltage-insensitive d (*lower abscissa* and *open bars*, Eq. 4a). Exceptions E90D and E123A show opposite relationships; mean results ± SE from $3 \leq n \leq 9$ independent treatments of WT and nine mutants. (B) Intersection of $I(E)$ curves resulting from changes of substrate concentration (here H^+) at one side of the membrane; data and fits replotted from typical E90Q example, equivalent to E90Q5 in Fig. 4 E.

yielded clearly positive z_E values (see Table S1 and Fig. 5 A). E90H looks like an intermediate with $z_E \approx 0$, and no significant (2 out of 3 trials) preference for the elastic voltage divider (see Table S1). (The time-consuming fits with the elastic potential profile were only performed for quantitative purposes, e.g., for Figs. 2 C, 4, 6, and Table S1. For demonstrations of simply qualitative issues (e.g., Figs. 3 B and 5 B), the faster fit routine with a rigid potential profile was applied.)

Inspection of the sets of six $I(E)$ curves from 10 different ChR2 in Fig. 4 allows the following notations. Most sets display similar shapes of the $I(E)$ curves with striking inward rectifying characteristics in the presence of 100 mM external Na^+, and much smaller and more linear currents in the absence of external Na^+, especially at alkaline pH_e when the H^+ contribution is small. E90H is the only mutant that shows a very small Na^+ contribution (Fig. 4 D). In all other mutants, there are strong inward currents in the presence of external Na^+ (*solid symbols*), but they show markedly different pH_e sensitivities. Whereas a $[H^+]_e$-induced stimulation of the conductance is observed in E90D, E90H, E123A, and E123T, an inhibition is noticed in E90Q, H134R, and H134S, and nonmonotonic changes in WT, E123Q, and T159C. Exceptional are the decreasing slopes for larger negative voltages in the $I(E)$ curves of E123A in neutral and even more in acidic pH_e; these extra wiggles appeared in all cells tested and correlate with the positive z_E in this mutant (Table S1, Fig. 5 A). Most of the substitutions tested cause a general decrease of the conductance (only H134R and T159C show similar or larger conductance than WT). This finding might indicate many sites that impede the ChR2-conductance in an unspecific way. However, the pronounced conductance increase in T159C does not support this view.

The numerical fit results of the z_E values and of the fundamental rate k^0 constants are compiled in Table S1 for the three best fits of each ChR. These results show fair numerical consistency of some parameters, and considerable scatter of some others. In some instances the large numerical values indicate degeneration of the general model toward one of the two simplifications of Fig. S1, B and C: large k^0_{ce} and k^0_{ec} as in WT, H134R, and T159C, reflect fast reorientation and high conductance (see Fig. 4), and large k^0_{Mc} and k^0_{Me} in WT, H134S, and T159C reflect fast binding equilibria for M^+. These patterns confirm that ChR2 does not correspond to either of the two simplifications (Fig. S1, B and C). The general model (Fig. 1 C) with finite rate constants (Table S1) seems to be appropriate in most instances, especially with respect to the well-reproduced parameters, such as z_E.

No obvious relationship was found between the apparent charge z_E of the empty binding site and the charge of the substituted amino acid of the particular mutants. In most cases z_E is around -0.3, irrespective of replacing the acidic Glu by neutral His, Gln, or Thr. Similarly, replacing the

weakly basic His[134] by the strong basic Arg or the neutral Ser did not affect $z_E \approx -0.3$. Clearly, positive z_E was found only in E123A. This finding is related to the striking and consistent wiggle at pH_c 6, which is interpreted by the model as the initiation of negative slope toward more negative voltages, i.e., a characteristic feature, when the empty binding site and the loaded one have the same sign of the charge (12). Approximately neutral $z_E \approx 0$ was found only in E90D (for unknown reasons) and in E90H, which has exceptionally small inward currents at basic and neutral pH_e. We conclude that alone the electric charge of the substitutes is insufficient to account for the apparent charge z_E of the empty binding site. The exact position of this charge in its local environment and the structure of the substitute seem to be more critical.

Fast and asymmetric reorientation equilibrium of empty site

One consistent result through all ChRs is $k_{ec}^0 >> k_{ce}^0$ (Table S1 and Fig. S3), which means that the empty binding has a strong orientation preference to the cytoplasmic side in the absence of a gradient. Together with the predominant charge number $z_E \approx -0.3$ (i.e., charge of the loaded site $\approx +0.7$), this finding might suggest that for large voltage displacements from equilibrium, k_{ec} and k_{ce} become rate limiting, respectively, because of their weaker voltage-sensitivity compared to the reorientation of the loaded site, whereby k_{ec} would limit the outward current and k_{ec} the inward current. In our case of $k_{ec}^0 >> k_{ce}^0$ this mechanism would predict outward rectification, which is obviously not the case.

This paradox is solved by two arguments: i), the reorientation of the loaded site does not have the full voltage-sensitivity of $+0.7$, because of its partitioning in two serial steps; and ii), more effective, in case of increased k_{ec}^0, the fundamental rate constant k_{eS}^0 will increase proportionally; and this rate constant, does not show up explicitly in the list of independent parameters in Table S1, because of Eq. 1. However, this k_{eS}^0 is critical for inward current by all cation species because it represents external uptake; and a large k_{ec}^0 only mirrors this scenario for inward rectification.

Intersections of I(E) curves from different substrate concentrations at one side

It was pointed out that changes of the ionic transportee concentration at one side of the membrane will never yield an intersection between the old $I(E)$ and the new one (29). However, several cases are found in the collection of $I(E)$ curves in Fig. 4, where this statement is violated. This feature is highlighted by Fig. 5 B.

The obvious intersections of the experimental $I(E)$ curves at about -20 mV do not have to be assigned to unknown, allosteric pH effects, because the fits already do account for these relationships. The solution of the problem is competition of different substrates (here Na^+ and H^+) for the binding site. Protons inhibit the Na^+ current and are

conducted as well. Due to a saturation scenario in ChR2-E90Q (and the two H123 mutants), rising external H^+ causes augmented occupation of the binding site without proportional H^+ translocation. The result is a reduced availability of empty binding sites for Na^+ import. This causes suppression of the (Na^+) conductance at increasing $[H^+]_e$. This phenomenon can also be described by the reduced models mentioned (fits not shown), which equally comprise competition of various substrates for the empty binding site.
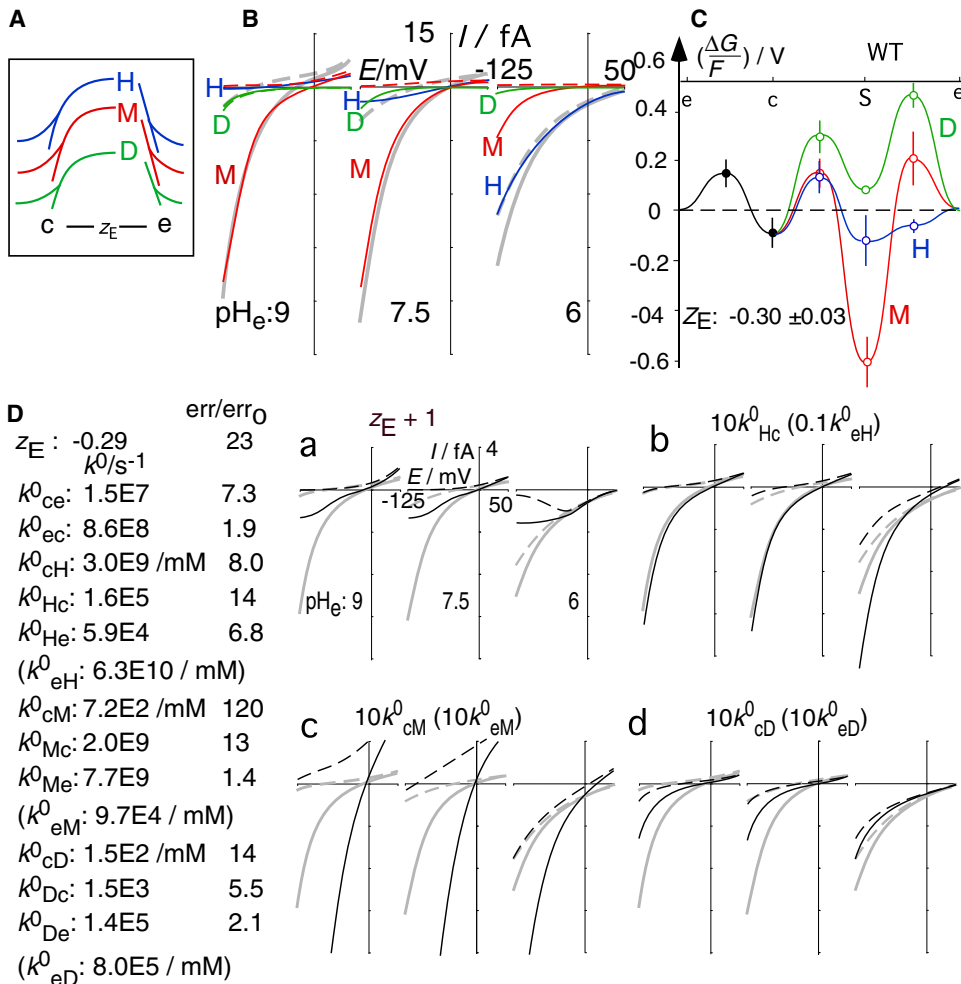
H-, M-, and D-components of total current

The total calculated currents in Fig. 4 comprise individual current components carried by the three ionic substrates H, M, and D. These individual components are shown in color for WT by Fig. 6 B and for all mutants (and WT) in Fig. S2; the ion-specific currents add up to the total current, which is marked in bold gray. In general, these current components match the intuitive expectations: i), the large inward currents at alkaline and even neutral pH_e are mostly carried by Na^+, if available outside; only in E90H, the Na^+ inward current amounts to <30% of the total current at neutral pH_e at -100 mV; ii), at pH_e 6, the inward currents are mostly carried by H^+; iii), in Na^+-free bathing solutions (*dashed curves*), the inward currents at alkaline pH_e are carried by D (Ca^{2+}); this finding means that D^{2+}—like H^+ in E90Q—acts in ChR2 not only as a blocking agent as in many channels but also as transportee; iv), the outward currents are mostly carried by M—mostly by K^+ because of high K^+ and low Na^+ in the cytoplasm. The apparent inhibition of conductance by external H, as shown in Fig. 5 B, is readily identified as an inhibition of the M conductance in the E90Q example, where the inward current at pH_e 6 comprises only a small M component. This pattern is present in all panels more or less explicitly, when the M inward currents are compared between pH 7.5 and pH 6 (also in Fig. 6 B). The opposite effect (stronger M inward currents at more acidic pH_e), is only found to a weak extent between pH_e 9 and 7.5 in WT, E90D, E123A, E123T, and T159C (Fig. S2).

Potential profiles

The numerical results from Table S1 can be illustrated by potential profiles at the same place, as shown by Fig. S3. For uniport of one arbitrary substrate S through one three-state cycle of the general model in Fig. 1 C illustrates the conversion of a given set of six rate constants to a potential profile with three barriers and three troughs e, S, and c, between them. The key relationship for this conversion is Eq. 2. For the energy profiles we did not use the fundamental rate constants k^0 at physical reference conditions (zero voltage and all concentrations 1 mM) but at our physiological reference conditions (also zero voltage but $pH_c = pH_e = 7.5$, $M_c = M_e = 100$ mM, and $D_c = D_e = 2$ mM).

FIGURE 6 Evaluation. (*A*) Reaction scheme of general model for translocation of H^+, M^+, and D^{2+} through ChR2. (*B*) Dissection of total fitted WT currents (*bold gray*) from Fig. 4 *B* in components carried by H, M, and D. Equivalent plots for the 0 mutants (and WT) are given by Fig. S2. (*C*) Potential profiles for ion conductance of WT ChR2; means from three best fits (Table S1); error bars: $\pm$SE; arbitrary reference zero level e: empty site oriented to external side; corresponding profiles from all nine mutants (and WT) and scheme for conversion of rate constants to potential profile are given in Fig. S3. (*D*) Major impact of independent model parameters z_E, k^0_{Hc}, k^0_{cM}, and k^0_{cD} on $I(E)$, demonstrated by example E123Q1 (Fig. 2, fitted model parameters from Table S1), showing theoretical changes of $I(E)$ upon a 10-fold increase of an individual parameter (concomitant k^0_{eS} values in brackets) in black; reference (*bold gray*) with (*solid*) and without (*dashed*) external Na^+. Column err/err$_0$ of inset table: relative increase of mean deviation from experimental data, indicating the respective impact of the given parameter on the ChR2 $I(E)$. A survey for all parameters is given by Fig. S3.

Some general features for ChR2 can be identified in these profiles (Fig. 6 *C* and Fig. S3):

1. As mentioned already, the position of the second black point from the left below zero ($k^0_{ec} > k^0_{ce}$) means that the empty binding site is mainly oriented toward the cytoplasmic side in the absence of a gradient, and—more important—the concomitant binding of external substrate (k^0_{eS}) is fast.
2. In physiological conditions, the limiting barrier for H^+ translocation is usually the cytoplasmic one (except E90H and E90Q), for M translocation it is the external one (except in E90H, E90D, and H134R), and for D it is also the external one with the exception of E90H.
3. The instances of very low external barrier (especially for H in WT, E123Q, H123R, and T159C) indicate configurations that might be described equally well with the simpler, fast-binding model, however not in general but only with respect to a specific substrate (here H), whereas a different substrate (here D) may simultaneously show slow binding equilibria in the very section.

4. Similar to electric circuitry, if serial barriers have different altitudes (resistances), the order of the barriers is irrelevant for the overall $I(E)$ relationship in general. However, specific assignments are possible, e.g., due to local changes in substrate concentration, as done here.
5. It might be questioned, why the conductance of E90H (Fig. S3) is so low, although the barriers are very small. The low energy troughs of the binding site provide the answer. When the site is mostly occupied, there are only a few empty sites available for accepting transportees.

It should be recalled that this kinetic analysis does not consider the important dependence on the light-sensitivity of ChR2, as all data are not only related to a fixed light intensity but even to a specific state, O_1, within the photocycle. However, because the state O_1 is the predominant conducting state at low light intensities or upon flash stimulation, the conclusions drawn here are most valuable for these conditions. The cycle in C_1-O_1 (Fig. 1 *A*) should not be mixed up with the transport cycle of the enzyme in state O_1 (Fig. 1 *C*), and thus light intensity has only a parametric influence on the rate constants of Fig. 1 *C*.

Impact of individual parameters

Fig. 6 D illustrates the major influence of four independent parameters (z_E, k_{Hc}^0, k_{cM}^0, and k_{cD}^0) of the general model on the ChR2 $I(E)$. The analysis of the experiment E123Q1 with the listed parameter values from the best fit, serves as a reference. The right column err/err$_0$ in the inserted table indicates the relative impact of each independent parameter on the ChR2 $I(E)$, which is confirmed by the four examples shown by the graphs. It is recalled that single changes of a fundamental rate constant are coupled to a concomitant change in k_{Se}^0 because of $k_{eS}^0 = k_{Se}^0 k_{ec}^0 k_{cS}^0 / (k_{Sc}^0 k_{ce}^0)$, i.e., in case of a change in k_{ce}^0 or k_{ec}^0, all three k_{eS}^0 values change concomitantly as well, as marked in brackets.

Fig. S4 shows this relative impact not only for the four parameters given in Fig. 6 D but for all of them. In summary, the parameters with the greatest impact on $I(E)$ of the reference configuration are z_E for the shape of the $I(E)$ curves, and the binding rate constant(s) k_{cM} (k_{eM}) for scaling of the predominant M currents. Thus, for a significant improvement of the Na$^+$ conductances and to depolarize membranes with lower light intensity, this binding affinity should be improved.

Rectification

Inward rectification of ChR-2 is undisputed as such. Initially, voltage gating was anticipated in analogy to many ion channels. Alternatively, Berthold et al. (25) suggested an enzyme kinetic model with fast binding equilibria (Fig. 2 D, left and Fig. S1 B) for ChR, which does not employ a voltage dependent function $a(E)$ of the activity, but operates with a voltage-dependent transport function, different from GHK. Furthermore, Feldbauer et al. (8) suggested that the nonlinearity of the steady-state $I(E)$ relationship of WT ChR-2 is an intrinsic feature of the transport function due to an asymmetric barrier. Diekmann et al. have worked out this approach for a synthetic channel (30). However, Fig. 2 B shows that this approach does not satisfy the $I(E)$ results.

For understanding the rectification mechanism in ChR2 we focus on symmetric scenarios with no concentration gradients (all reversal voltages are zero), and assume simple configurations with a maximum of two different substrates of $z_S = +1$ and rounded parameter values (Fig. 7).

For the sake of clarity, the ordinates in these diagrams are simple turnover numbers J in s^{-1}. With calculated $J(E)$ curves from these schematic reaction cycles, possible mechanisms of rectification can be identified, and other possibilities can be excluded. Within our context, we treat inward rectification here explicitly. Corresponding considerations apply for outward rectification.

Fig. 7 A illustrates translocation of a single substrate A through the general model. Configuration a serves as a reference with symmetrical, sigmoid $J(E)$ and no rectification. In
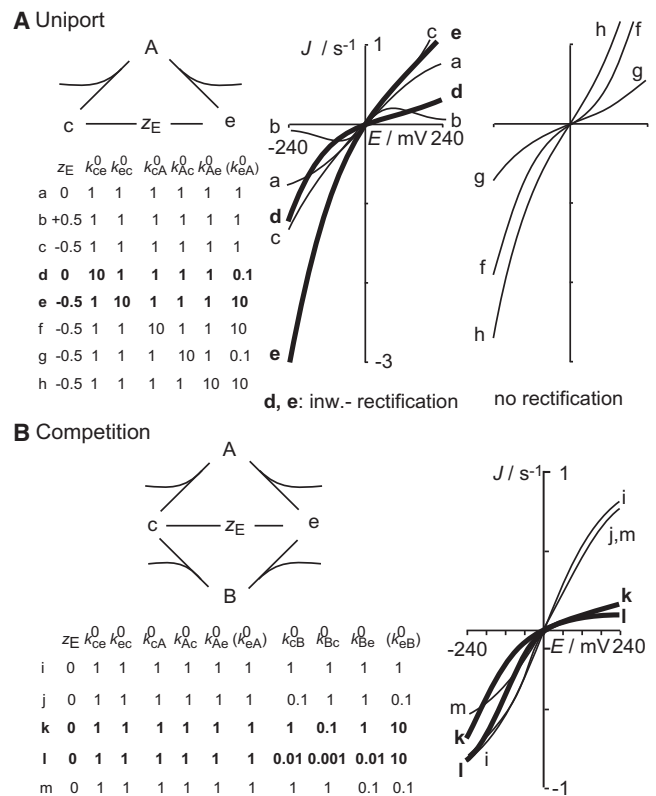
A Uniport

z_E	k_{ce}^0	k_{ec}^0	k_{cA}^0	k_{Ac}^0	k_{Ae}^0	(k_{eA}^0)
a	0	1	1	1	1	1	1
b	+0.5	1	1	1	1	1	1
c	-0.5	1	1	1	1	1	1
d	0	10	1	1	1	1	0.1
e	-0.5	1	10	1	1	1	10
f	-0.5	1	1	10	1	1	10
g	-0.5	1	1	1	10	1	0.1
h	-0.5	1	1	1	1	10	10

d, e: inw.- rectification   no rectification

B Competition

z_E	k_{ce}^0	k_{ec}^0	k_{cA}^0	k_{Ac}^0	k_{Ae}^0	(k_{eA}^0)	k_{cB}^0	k_{Bc}^0	k_{Be}^0	(k_{eB}^0)
i	0	1	1	1	1	1	1	1	1	1	1
j	0	1	1	1	1	1	1	0.1	1	1	0.1
k	0	1	1	1	1	1	1	1	0.1	1	10
l	0	1	1	1	1	1	1	0.01	0.001	0.01	10
m	0	1	1	1	1	1	1	1	1	0.1	0.1

FIGURE 7 Schematic mechanisms for inward rectification in ChR2 via general model in Fig. 1 C; numerically listed scenarios do not only show the independent, fundamental rate constants but also the dependent ones, k_{eA}^0 and k_{eB}^0. (A) (Uniport of one substrate A): from the listed parameter configurations, only scenarios **d** and **e** cause inward rectification. (B) Inward rectifying impact of competing substrate B on A currents (*bold*) through symmetric uniport configuration, no matter if substrate B is translocated in major (*scenario* **k**) or minor (*scenario* **l**) amounts; all other configurations listed cause no rectification or weak outward rectification (m).

case of $z_E = 0$, k_{ec} and k_{ce} are voltage-insensitive and determine the saturation currents at large voltage displacements from equilibrium by their values k_{ec}^0 and k_{ce}^0, respectively.

Introducing a charge $z_E \neq 0$ to the empty binding site (case b and c), is not sufficient for an asymmetry of the $J(E)$ curves. However, $z_E \neq 0$ severely affects the saturation behavior, forming exponentially falling (b) or rising (c) currents for large voltage displacements.

As mentioned, configuration **d** in Fig. 7 A shows inward rectification with $z_E = 0$, when the different, voltage-insensitive k_{ce}^0 and k_{ec}^0 determine the large negative saturation rate of 10 s^{-1} (outside given voltage window) and the small positive one (1 s^{-1}, not visible either), respectively. With $z_E = -0.5$, however, only configuration **e** with $k_{ec}^0 > k_{ce}^0$ seems to yield pronounced inward rectification. Meanwhile, we know that it is not the small k_{ce}^0 itself that is critical for inward rectification in Fig. 7 A, but the concomitant, large k_{eS}^0 for external cation uptake. Therefore, given an experimentally determined $z_E \approx -0.3$ in ChR, this scenario **e** reflects the predominant mechanism for rectification in ChR2 uniport.

Alternative changes in the reaction section of the loaded site (k_{cA}^0, k_{Ac}^0, and k_{Ae}^0) by the scenarios f, g, and h, do not lead to $I(E)$ asymmetries, because of the concomitant changes in k_{eA}^0. It is pointed out in particular, that barriers of unequal heights (scenario h in Fig. 7 A) do not infer rectification as such. The corresponding, symmetric $I(E)$ relationship rather means again, that the order of the serial barriers is irrelevant for the total $I(E)$ relationship.

Fig. 7 B shows the possibly rectifying effect of a competing substrate B on a nonrectifying reaction system for the primary substrate A. Scenario i serves as a symmetric reference here. A reduction in k_{cB}^0 (configuration j) has virtually no effect on the $I(E)$. However, a decrease of k_{Bc}^0 by factor 10 causes significant inward rectification, no matter whether the secondary substrate is transported in major, stoichiometric amounts (scenario **k**), or acts in minor, catalytic amounts (scenario **l**). This decrease of k_{Bc}^0 causes affinity increases, k_{cB}^0/k_{Bc}^0 and k_{eB}^0/k_{Be}^0 for B at both sides, but with a faster binding equilibrium to the external medium due to the concomitant increase of k_{eB}^0 than to the cytoplasmic one. A corresponding change in k_{Be}^0 (scenario m) causes no affinity changes, and only a weak outward rectification.

CONCLUSIONS

The nonlinear current-voltage relationships of the early state O_1 in the photocycle of WT and nine mutants of ChR2, as recorded in various bath media, are analyzed in reaction kinetic terms by a model with one predominant binding site that carries an apparent charge of about -0.3 in its empty state.

The mechanism for ChR2 inward rectification consists of intrinsic rectification by the uniport function, plus competitive inhibition from outside.

Ion transport across serial barriers follows the concept of a voltage-sensitive, elastic voltage divider.

SUPPORTING MATERIAL

Detailed descriptions of the numerical treatment of the five transport models used and the applied fitting strategy, equations, four figures, a table, and references (31–34) are available at http://www.biophysj.org/biophysj/supplemental/S0006-3495(11)00898-8.

REFERENCES

1. Hegemann, P. 2008. Algal sensory photoreceptors. *Annu. Rev. Plant Biol.* 59:167–189.

2. Schoenenberger, P., Y. P. Schärer, and T. G. Oertner. 2011. Channelrhodopsin as a tool to investigate synaptic transmission and plasticity. *Exp. Physiol.* 96:34–39.

3. Baker, M. 2011. Light tools. *Nat. Methods.* 8:19–22.

4. Hegemann, P., S. Ehlenbeck, and D. Gradmann. 2005. Multiple photocycles of channelrhodopsin. *Biophys. J.* 89:3911–3918.

5. Nikolic, K., N. Grossman, …, P. Degenaar. 2009. Photocycles of channelrhodopsin-2. *Photochem. Photobiol.* 85:400–411.

6. Nikolic, K., P. Degenaar, and C. Toumazou. 2006. Modeling and engineering aspects of channelrhodopsin2 system for neural photostimulation. *Conf. Proc. IEEE Eng. Biol. Soc.* 1:1626–1629.

7. Harz, H., C. Nonnengasser, and P. Hegemann. 1992. The photoreceptor current of the green-alga *Chlamydomonas. Philos. Trans. R. Soc. Lond. Ser. B.* 338:39–52.

8. Feldbauer, K., D. Zimmermann, …, E. Bamberg. 2009. Channelrhodopsin-2 is a leaky proton pump. *Proc. Natl. Acad. Sci. USA.* 106:12317–12322.

9. Lin, J. Y., M. Z. Lin, …, R. Y. Tsien. 2009. Characterization of engineered channelrhodopsin variants with improved properties and kinetics. *Biophys. J.* 96:1803–1814.

10. Lu, Z. 2004. Mechanism of rectification in inward-rectifier K^+ channels. *Annu. Rev. Physiol.* 66:103–129.

11. Andersen, O. S. 1989. Kinetics of ion movement mediated by carriers and channels. *Methods Enzymol.* 171:62–112.

12. Gradmann, D., and C. M. Boyd. 2005. Apparent charge of binding site in ion-translocating enzymes: kinetic impact. *Eur. Biophys. J.* 34:353–357.

13. Roux, B. 2005. Ion conduction and selectivity in K(+) channels. *Annu. Rev. Biophys. Biomol. Struct.* 34:153–171.

14. Gradmann, D., H. G. Klieber, and U. P. Hansen. 1987. Reaction kinetic parameters for ion transport from steady-state current-voltage curves. *Biophys. J.* 51:569–585.

15. Nagel, G., T. Szellas, …, E. Bamberg. 2003. Channelrhodopsin-2, a directly light-gated cation-selective membrane channel. *Proc. Natl. Acad. Sci. USA.* 100:13940–13945.

16. Tsunoda, S. P., and P. Hegemann. 2009. Glu-87 of channelrhodopsin-1 causes pH-dependent color tuning and fast photocurrent inactivation. *Photochem. Photobiol.* 85:564–569.

17. Berndt, A., M. Prigge, …, P. Hegemann. 2010. Two open states with progressive proton selectivities in the branched channelrhodopsin-2 photocycle. *Biophys. J.* 98:753–761.

18. Gunaydin, L. A., O. Yizhar, …, P. Hegemann. 2010. Ultrafast optogenetic control. *Nat. Neurosci.* 13:387–392.

19. Berndt, A., P. Schoenenberger, …, T. G. Oertner. 2011. High-efficiency channelrhodopsins for fast neuronal stimulation at low light levels. *Proc. Natl. Acad. Sci. USA.* 108:7595–7600.

20. Ruffert, K., B. Himmel, …, V. Eulenburg. 2011. Glutamate residue 90 in the predicted transmembrane domain 2 is crucial for cation flux through channelrhodopsin 2. *Biochem. Biophys. Res. Commun.* 410:737–743.

21. Facciotti, M. T., S. Rouhani, …, R. M. Glaeser. 2001. Structure of an early intermediate in the M-state phase of the bacteriorhodopsin photocycle. *Biophys. J.* 81:3442–3455.

22. Zhang, F., M. Prigge, …, K. Deisseroth. 2008. Red-shifted optogenetic excitation: a tool for fast neural control derived from *Volvox carteri. Nat. Neurosci.* 11:631–633.

23. Neher, E. 1992. Correction for liquid junction potentials in patch clamp experiments. *Methods Enzymol.* 207:123–131.

24. Barish, M. E. 1983. A transient calcium-dependent chloride current in the immature *Xenopus* oocyte. *J. Physiol.* 342:309–325.

25. Berthold, P., S. P. Tsunoda, …, P. Hegemann. 2008. Channelrhodopsin-1 initiates phototaxis and photophobic responses in *chlamydomonas* by immediate light-induced depolarization. *Plant Cell.* 20:1665–1677.

26. Nagel, G., D. Ollig, …, P. Hegemann. 2002. Channelrhodopsin-1: a light-gated proton channel in green algae. *Science.* 296:2395–2398.

27. Woodhull, A. M. 1973. Ionic blockage of sodium channels in nerve. *J. Gen. Physiol.* 61:687–708.

28. Hagedorn, R., D. Gradmann, and P. Hegemann. 2008. Dynamics of voltage profile in enzymatic ion transporters, demonstrated in electrokinetics of proton pumping rhodopsin. *Biophys. J.* 95:5005–5013.

29. Blatt, M. R. 1986. Interpretation of steady-state current-voltage curves: consequences and implications of current subtraction in transport studies. *J. Membr. Biol.* 92:91–110.

30. Dieckmann, G. R., J. D. Lear, …, K. A. Sharp. 1999. Exploration of the structural features defining the conduction properties of a synthetic ion channel. *Biophys. J.* 76:618–630.

31. Hansen, U. P., D. Gradmann, …, C. L. Slayman. 1981. Interpretation of current-voltage relationships for "active" ion transport systems: I. Steady-state reaction-kinetic analysis of class-I mechanisms. *J. Membr. Biol.* 63:165–190.

32. Hill, T. L. 1966. Studies in irreversible thermodynamics. IV. Diagrammatic representation of steady state fluxes for unimolecular systems. *J. Theor. Biol.* 10:442–459.

33. Nelson, P. H. 2011. A permeation theory for single-file ion channels: one- and two-step models. *J. Chem. Phys.* 134:165102–165113.

34. Hookes, R. T., and T. Jeeves. 1961. Direct search solution of numerical statistical problems. *Assoc. Comput. Mach.* 8:212–229.